RSC Chemical Biology

PAPER

Check for updates

Glyco-functionalization of ECM mimics, influence in morphology and cell behaviour

Maddalena Bracchi,[a] Francesco Nicotra[a] and Laura Russo ⓘ ⋆[abc]

Current tissue engineering strategies primarily focus on replicating mechanical properties of the extracellular matrix (ECM); however, several studies have underscored the critical role of the ECM biochemical cues in developing functional tissue substitutes. Among these, glycans are known to play a key role in regulating cell fate. In this study we developed ECM mimics glyco-conjugated with two different glycans, α-D-glucopyranose (αGlc) and β-D-galactopyranose (βGal), to investigate their influence on morphology and cell behaviour. The ECM mimics were generated crosslinking glycosylated gelatin samples, functionalised with the glycans by reductive amination, and hyaluronic acid. The crosslinking was performed by previous functionalization of gelatin and hyaluronic acid with tyramine, to enable enzymatic phenol-phenol coupling *via* horseradish peroxidase (HRP) and hydrogen peroxide (H_2O_2). The glyco-conjugated hydrogels exhibited markedly different morphologies, characterized by increased fibrous content, smaller pore sizes, and more wrinkled surfaces. Bone marrow-derived mesenchymal stem cells (BM-MSCs) seeded in hydrogels functionalized αGlc and βGal exhibited a more elongated morphology and differential glycosignature compared to controls.

Introduction

Extracellular matrix (ECM) mimetics[1] are gaining great interest not only for regenerative medicine purposes, but also to reproduce pathological tissues for animal-free drug screening, according with the most recent FDA guidelines,[2] and to identify biomarkers and morphological changes inducing pathological events. ECMs are hydrogels consisting of three-dimensional, hydrophilic polymer networks with strong swelling properties which allow to create an ideal cell microenvironment. Besides that, correct cell adhesion properties are required for their survival. To meet these requirements, a combination of polysaccharides providing swelling properties, and structural proteins to guarantee cell adhesion, are crosslinked to generate a suitable 3D network depending on the application. However, the cells need instructions to proliferate and differentiate generating the required tissue. It is now clear that not only the morphology and physical properties of the cell microenvironment provide cell signalling, but also, and more important, some signalling molecules. Indeed, the ECM is a dynamic environment that employs both biophysical and biochemical signals to regulate biological responses and maintain tissue function. Therefore, materials used in regenerative medicine must possess not only appropriate mechanical but also relevant biochemical properties to support tissue development and functionality. Among the various signalling molecules, glycans play a fundamental role in regulating tissue development and cell fate and pathological events induction.[3,4] For this reason, accurately replicating the native glycosignature in tissue engineering scaffolds is essential to ensure proper osteochondral and meniscal tissue regeneration and function.

Results and discussion

In this study we developed ECM mimics, based on covalently crosslinked gelatin and hyaluronic acid, and functionalised with two different glycans: α-D-glucopyranose (αGlc) and β-D-galactopyranose (βGal). Gelatin was selected for its favourable properties, including biocompatibility, biodegradability, low immunogenicity, and the presence of Arg-Gly-Asp (RGD) motifs that promote cell adhesion. Moreover, it is derived from denatured collagen, the primary structural component of the ECM. Hyaluronic acid, a non-sulfated glycosaminoglycan (GAG), was used due to its key characteristics, such as viscoelasticity, water-retention capacity, and its role in modulating inflammation.

As glycans, αGlc and βGal were selected due to their presence in the ECM collagen, Glc(α1-2)Gal(β1-O) is bound to hydroxylysine across collagens to mammals,[5] and collagen

[a] *School of Medicine and Surgery, Università degli Studi di Milano-Bicocca, Monza, Italy*

[b] *Fondazione IRCCS San Gerardo dei Tintori, Monza, Italy*

[c] *CURAM Research Ireland Centre for Medical Devices, University of Galway, Galway, Ireland*

© 2025 The Author(s). Published by the Royal Society of Chemistry

RSC Chem. Biol., 2025, **6**, 1893–1908 | 1893

glycosylation modulates its structure and functions.[6] Furthermore, dysregulation of collagen glycosylation impacts in pathological events such as diabetes[7] and cancer.[4] Additionally, we selected chondroitin sulfate, a sulphated GAG with multifarious role in the ECM, such as its remodelling,[8] angiogenesis,[9] regulation of immunity.[10]

To perform the covalent crosslinking, both gelatin and hyaluronic acid were functionalised with tyramine to allow an enzymatic oxidative phenol–phenol coupling with H_2O_2 catalysed by horseradish peroxidase (HRP).[11]

Covalent functionalization of gelatin with glycans

The glycans were separately attached to gelatin *via* a reductive amination of the aldehyde at the anomeric centre of the reducing sugar and the primary amino groups of the lysine residues of gelatin. In this reaction, occurring with $NaBH_3CN$ at pH 5.5, the pyranosidic structure of the reducing sugar is lost, providing an open chain alditol. Therefore, to functionalise gelatin respectively with αGlc and βGal, we exploited respectively maltose [Glcα(1–4)Glc] and lactose [Galβ(1–4)Glc], in the reductive amination the reducing monosaccharide (Glc) loses its pyranosidic structure and acts as a linker, whereas the αGlc and βGal units are preserved (Scheme 1). The synthetic procedure was adapted from previous works.[12,13] Briefly, gelatin (500 mg, 2% w/V) was dissolved in 0.1 M MES pH 5.5 buffer at 37 °C. Then maltose or lactose (6 g, 24% w/V), were added to the solution and stirred for 30 min. Subsequently, 586 mg of $NaBH_3CN$ were added, and the mixture was left under stirring for 2 h 30 min.

Covalent functionalization of gelatin and hyaluronic acid with the tyramine

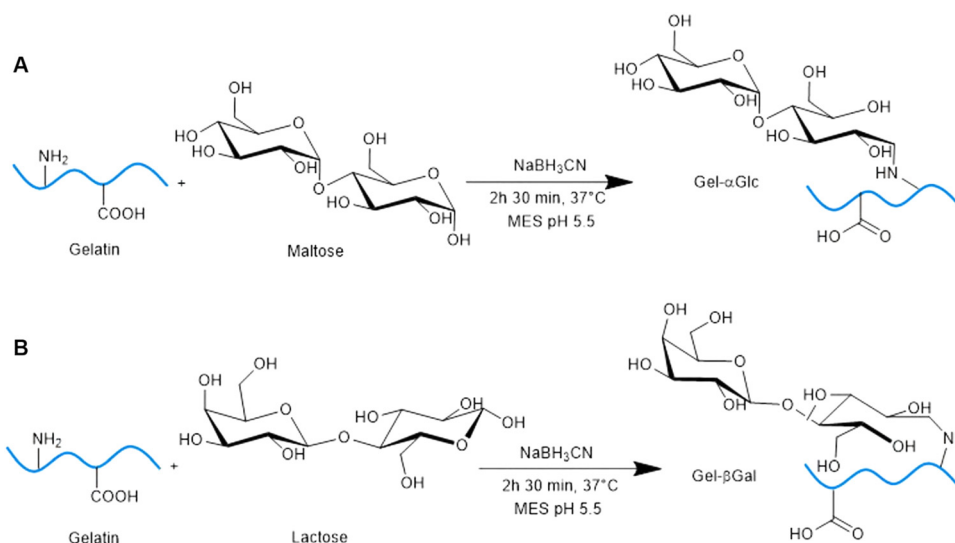Gelatin functionalised with tyramine (Gel-Tyr) and hyaluronic acid functionalised with tyramine (HA-Tyr) were synthesized using the protocol described in a previous work[14] and illustrated below (Scheme 2).

As previously reported,[14] for HA-Tyr, hyaluronic acid (500 mg, 1% w/V) was dissolved in 0.1 M MES pH 5.5, then 253 mg EDC and 152 mg NHS were added, and the solution was stirred for 40 min. Then tyramine (181 mg, 0.9% w/V) dissolved in 0.1 M MES pH 5.5 was added dropwise. After 40 min, again 253 mg EDC and 152 mg NHS were added to the reaction, which was allowed to proceed under mild stirring overnight. HA-Tyr functionalization was confirmed through FTIR, ^{1}H-NMR and UV-VIS characterizations (SI).

For Gel-Tyr (2 g, 2% w/V), the same procedure was followed, using gelatin instead of hyaluronic acid.[14] Briefly, 77 mg of EDC and 46 mg of NHS were added to solution and stirred for 40 min. Tyramine (55 mg, 0.9% w/V) was dissolved in 0.1 M MES pH 5.5 and added dropwise. After 40 min, again 77 mg EDC and 46 mg NHS were added to the reaction, which was allowed to proceed under mild stirring overnight. The resulting products were finally dialyzed using a 14 kDa cellulose membrane for 24 h with 0.1 M NaCl solution and 48 h against deionized water, changing the dialysis solution four times per day. The same protocol was utilised to attach tyramine to gelatin already functionalised with αGlc and βGal, generating Gel-Tyr-αGlc and Gel-Tyr-βGal. Tyramine grafting was confirmed by FTIR spectroscopy (SI) in which the differences in peaks observed between 1620 and 1200 cm^{-1} in Gel-Tyr Gel-Tyr-αGlc and Gel-Tyr-βGal, suggesting the introduction of new functional groups or structural modifications in Gel after conjugation. The purified products were freeze-dried using Vacuum Freeze Dryer (Boyikang Laboratory Instruments Inc, Beijing, China) for 48 h at $T = -50$ °C and pressure below 15 Pa and stored at -20 °C until further use.
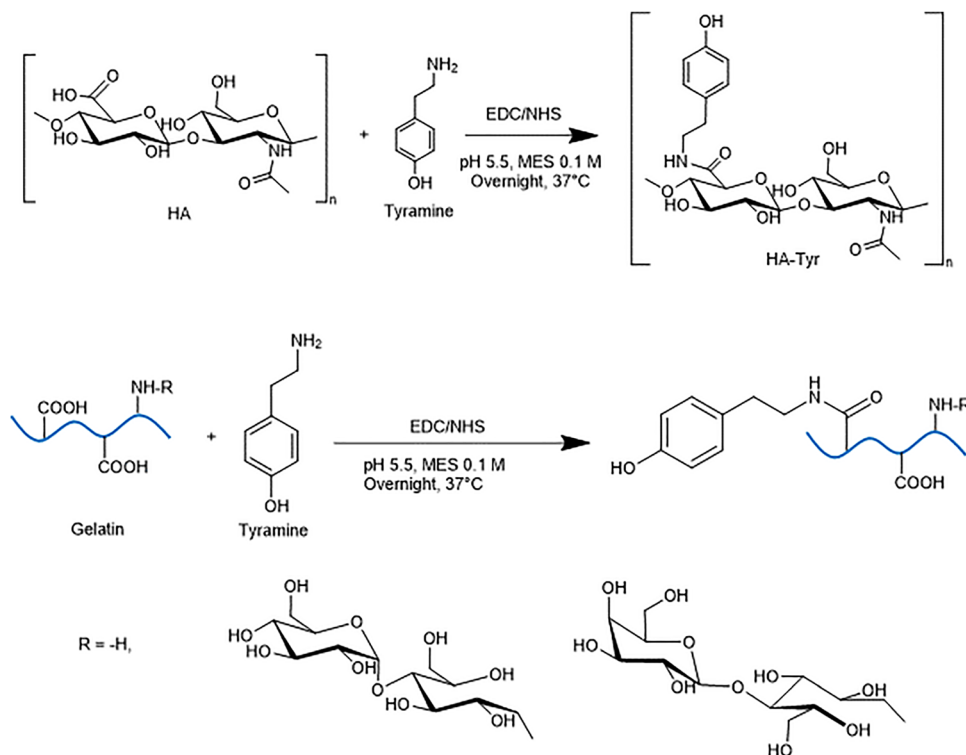
Quantification of the functionalization

^{1}H-NMR and UV-VIS analysis. ^{1}H-NMR was performed at 400 MHz on a Varian Mercury 400, with samples prepared by

Scheme 1 Functionalization of gelatin with αGlc ((A), Gel-αGlc) and βGal ((B), Gel-βGal) by reductive amination with maltose and lactose, respectively exploiting the lysine residues of the protein.

1894 | *RSC Chem. Biol.*, 2025, **6**, 1893–1908

© 2025 The Author(s). Published by the Royal Society of Chemistry

Scheme 2 Functionalization of hyaluronic acid (HA) and gelatin (Gel) with tyramine.

dissolving 5 mg of the product in 500 µL of D$_2$O. The lysine peak at 2.9 ppm and characteristic sugar peaks were studied to qualitatively confirm glycan conjugation. Furthermore, the degree of functionalization (DoF), defined as the ratio of the weight of phenol groups to the total product weight, was determined by comparing the integral ratio of the phenyl proton peaks of tyramine (6.85 and 7.19/7.17 ppm) to the TMSP reference peak integral (0 ppm). Fig. 1A shows the ^{1}H-NMR spectrum of Gel-Tyr-αGlc, compared to the spectra of Gel-Tyr and Gel. A decrease in the characteristic of –CH$_2$NH$_2$ peak lysine at 2.9 ppm is observed in both Gel-Tyr-αGlc and Gel-Tyr, in agreement with the conversion into a –CH$_2$NH– group as well as partial internal crosslinking between the amine and activated carboxylic groups of gelatin (pink band). Therefore, it cannot be used as a quantitative parameter for glycans conjugation. Furthermore, the presence of glucose in Gel-Tyr-αGlc is confirmed by its characteristic peak at 5.45 ppm in the functionalized sample (green band). Tyramine has two characteristic peaks at 6.85 ppm and 7.19/7.17 ppm, which are present in both Gel-Tyr-αGlc and Gel-Tyr (yellow bands). While Gel also shows some signal in this region due to its aromatic groups, these peaks are more pronounced in the functionalized materials. The DoF was determined by comparing the ratio of the integrated areas under the aromatic peaks to the reference peak of TMSP at 0 ppm, reaching 1.2% for Gel-Tyr and 1.0% for Gel-Tyr-αGlc. These data were consistent with the UV-VIS
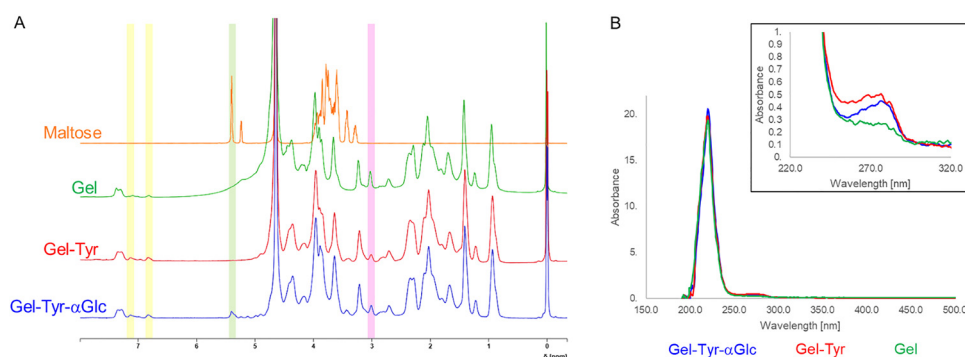

Fig. 1 ^{1}H-NMR spectra of Gel-Tyr-αGlc, Gel-Tyr, Gel, and maltose with highlighted main peaks (A), and UV-VIS graphs of Gel-Tyr-αGlc, Gel-Tyr, and Gel with a magnified view of the tyramine peak region (B). Notably, the peak at the tyramine level is comparable in Gel-Tyr-αGlc and Gel-Tyr but lower in Gel, confirming the successful grafting.
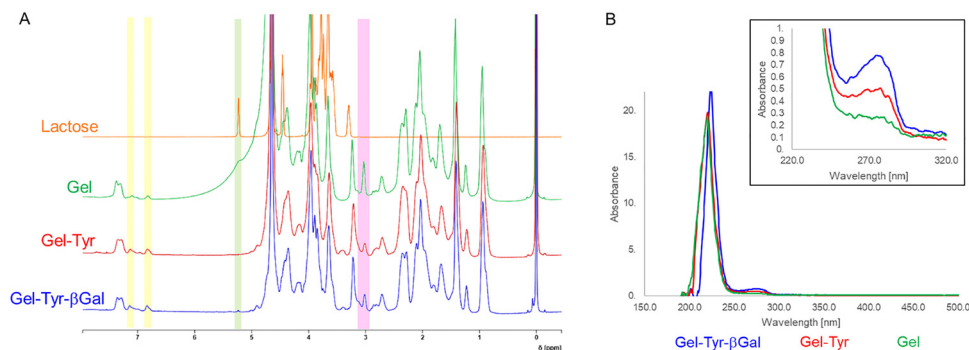
© 2025 The Author(s). Published by the Royal Society of Chemistry

RSC Chem. Biol., 2025, **6**, 1893–1908 | **1895**

Fig. 2 ^{1}H-NMR spectra of Gel-Tyr-βGal, Gel-Tyr, Gel, and Lactose with highlighted main peaks (A), and UV-VIS graphs of Gel-Tyr-βGal, Gel-Tyr, and Gel with a magnified view of the tyramine peak region (B). In this case, Gel-Tyr-βGal exhibits an even higher peak than Gel-Tyr, confirming that sugar conjugation does not impact the success of tyramine grafting.

analysis (Fig. 1B), where tyramine grafting was quantified at 0.75% for Gel-Tyr-αGlc and 0.70% for Gel-Tyr. In fact, the percentage of the amino acid tyrosine in gelatin, approximately 0.5%.[15]

A similar result was observed for Gel-Tyr-βGal. The ^{1}H-NMR analysis (Fig. 2A) showed a decrease in the lysine peak (pink band) and tyramine peaks (yellow bands) comparable to those in Gel-Tyr, resulting in a DoF of 1.1%. Additionally, lactose exhibits a peak at 5.4 ppm, which, although weak, is present in Gel-Tyr-βGal, confirming the conjugation. Furthermore, DoF of tyramine grafting from UV-VIS analysis was quantified as 0.8%, comparable with Gel-Tyr (Fig. 2B).

Colorimetric assays. The ninhydrin assay for primary amines was used to evaluate the amount of functionalised lysine with respect of the 5% in mass of lysine content in untreated gelatine. The functionalization resulted 2.80% for Gel-Tyr-αGlc and 2.75% for Gel-Tyr-βGal. However, these values reflect not only sugar conjugation but also partial internal crosslinking between the amine and activated carboxyl groups of aspartic and glutamic acid of gelatin. To specifically quantify the percentage of sugars in the samples, anthrone assay was performed. Calibration curves for maltose and lactose were obtained, and the percentage in mass in samples was calculated as 0.80% and 0.75% for Gel-Tyr-αGlc and Gel-Tyr-βGal, respectively. The molar DoF was 6.4%, 6.8% and 7.3% of carboxylic groups for Gel-Tyr, Gel-Tyr-αGlc and Gel-Tyr-βGal, respectively.
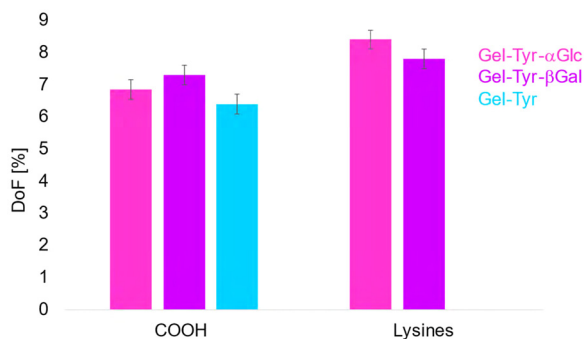
Correspondingly, the DoF relative to lysine residues was 8.4% for Gel-Tyr-αGlc and 7.8% for Gel-Tyr-βGal (Fig. 3).

Gelatin–hyaluronic acid crosslinking, hydrogels formulation

The hydrogels were formed via enzymatic crosslinking exploiting the oxidative phenol–phenol coupling with H_2O_2 catalysed by horseradish peroxidase (HRP) (Scheme 3).

This reaction occurs under mild conditions, aqueous solution, neutral pH, and physiological temperature, making it well-suited for biomedical applications.[16–18] The reaction was performed between HA-Tyr and the differently functionalised gelatins, Gel-Tyr, Gel-Tyr-αGlc and Gel-Tyr-βGal, defining the best experimental conditions.

Different formulations were designed starting from a previous study by modifying the relative amount of the starting materials (Table 1), while the concentrations of HRP and H_2O_2 were kept constant at 0.5 U mL^{-1} and 0.5 mM, respectively.[14] Freeze-dried materials were dissolved in D-PBS 7.4 at 37 °C until use, and the HRP and H_2O_2 solutions were prepared by dissolving stock solutions in deionized water to 12.5 U mL^{-1} and 0.01 M concentrations respectively. Hydrogels were prepared by mixing the respective materials, followed by the addition of HRP and, finally, H_2O_2 solutions.
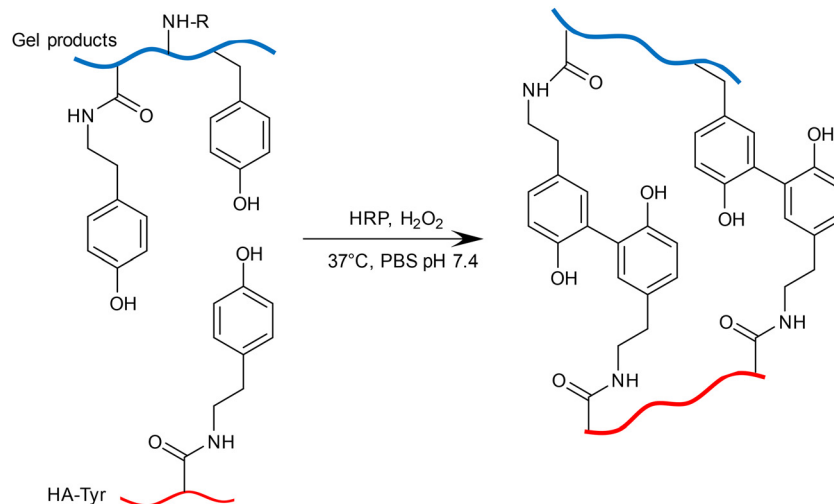
The gelation time of the hydrogels was measured using an inverting test in 2 mL Eppendorf tubes: a properly formed hydrogel stays at the bottom of the vial even after inversion. FTIR was also performed on freeze-dried samples to qualitatively confirm hydrogels formation.

In Fig. 4 the obtained spectra are displayed: crosslinked materials exhibit similar profiles, with slight variations due to the different conjugated sugars. Notable differences appear in the 1000–1200 cm^{-1} range particularly with the emergence of a 1030 cm^{-1} peak in crosslinked formulations, which may indicate successful crosslinking.

Furthermore, hydrogels formation was monitored through real-time UV-VIS, analysing three key stages: the solution blend before HRP addition, immediately after HRP addition but before activation, and the hydrogel formation right after H_2O_2 addition (SI).

The gelation time was monitored to assess whether sugar addition affects crosslinking kinetics (Table 2). It was observed

Fig. 3 Graph representing the molar DoF of lysines and carboxylic groups in Gel-Tyr-αGlc, Gel-Tyr-βGal and Gel-Tyr.

Scheme 3 Crosslinking reactions between functionalized Gel products and HA-Tyr achieved through an enzymatic HRP-mediated oxidation.

Table 1 Hydrogels formulations, obtained by combining HA-Tyr with Gel-Tyr-αGlc, Gel-Tyr-βGal or Gel-Tyr

Formulation	eq. mol phenols Gel-Tyr	eq. mol phenols HA-Tyr	c Gel-Tyr [mg mL^{-1} hydrogel]	c HA-Tyr [mg mL^{-1} hydrogel]
GelHA-0.30	1	0.30	26	4
GelHA-0.45	1	0.45	24	6

Formulation	eq. mol phenols Gel-Tyr-aGlc	eq. mol phenols HA-Tyr	c Gel-Tyr-aGlc, [mg mL^{-1} hydrogel]	c HA-Tyr [mg mL^{-1} hydrogel]
GelHA-0.30-αGlc	1	0.30	26	4
GelHA-0.45-αGlc	1	0.45	24	6

Formulation	eq. mol phenols Gel-Tyr-bGal	eq. mol phenols HA-Tyr	c Gel-Tyr-bGal [mg mL^{-1} hydrogel]	c HA-Tyr [mg mL^{-1} hydrogel]
GelHA-0.30-βGal	1	0.30	26	4
GelHA-0.45-βGal	1	0.45	24	6

that formulations with a higher HA-Tyr concentration exhibited faster crosslinking kinetics. Additionally, in formulations with the same molar equivalents, the conjugation of sugars on gelatin led to an increase in gelation time.

Hydrogels characterization

SEM analysis. Hydrogels for SEM analysis were prepared by freezing overnight at −20 °C, storing at −80 °C, and subsequently freeze-drying. The resulting images are shown in Fig. 5, while pore dimensions are provided in Table 3. It is evident that formulations containing sugar exhibit a totally different morphology compared to the control samples, with more fibres and smaller pores and a smoother and more wrinkled surface. Notable differences are present among these samples: formulations with αGlc are characterized by a more reticular structure, while samples containing βGal exhibit an intermediate behaviour between the other two. However, across all formulations, pore size remains highly variable due to the high SD, in particular in formulations without sugars, as well as in GelHA-0.45-αGlc and GelHA-0.30-βGal. One-way ANOVA was performed, which highlights significant differences between samples with and without sugar. A statistically significant

difference in porosity was observed between the sugar-conjugated formulations and the control hydrogels, indicating that the morphology undergoes changes as a result of this functionalization, regardless of the specific sugar used.

Rheological tests. An amplitude sweep test was performed to assess the rheological properties of the formulations, and the results are presented in Fig. 6A and Table 4. Formulations with a higher HA concentration exhibit higher G' values, while G'' increases only in the formulation without sugar and remains comparable in the others. G' values are significantly lower in formulations containing sugars compared to GelHA-0.30 and GelHA-0.45, which also show lower yield and flow points (γ_y and γ_F, respectively). Among the sugars, glucose results with the lowest G', while galactose leads to the highest. Overall, the addition of sugar enhances the viscous properties of the hydrogels.

Viscosity curves for the formulations are presented in Fig. 6B. All formulations exhibited shear-thinning behaviour, characterized by a decrease in viscosity with increasing shear stress. This pseudoplastic behaviour was modelled using the Power Law,[19] and the corresponding K and n parameters were determined (Table 5). Higher K values were observed in the GelHA-0.30-αGlc, GelHA-0.30-βGal, GelHA-0.45-αGlc, and

© 2025 The Author(s). Published by the Royal Society of Chemistry

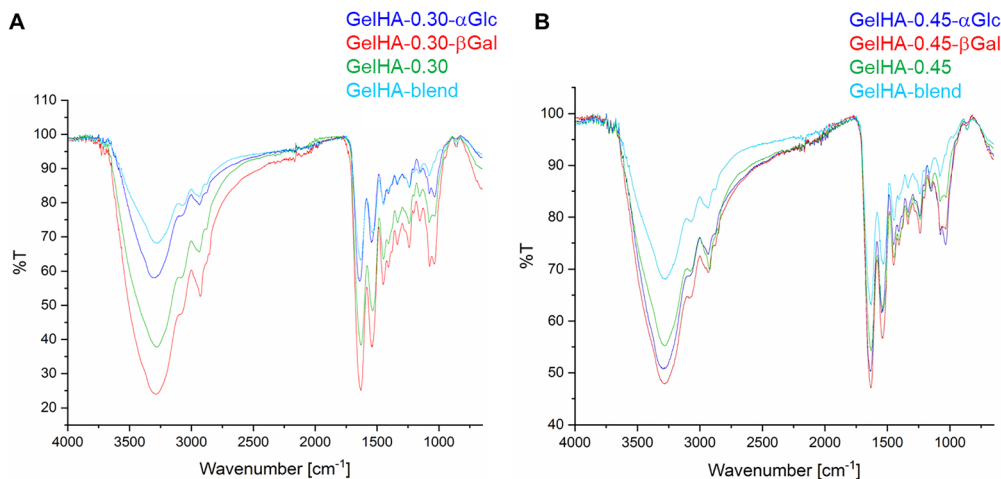*RSC Chem. Biol.*, 2025, **6**, 1893–1908 | **1897**

Fig. 4 FTIR spectra of Gel : HA = 1 : 0.30 (A) and Gel : HA = 1 : 0.45 formulations (B), compared to GelHA-blend.

Table 2 Gelation times of enzymatically crosslinked hydrogels formed with functionalized Gel and HA-Tyr

Formulation	Gel used	eq. phenols Gel-Tyr	eq. phenols HA-Tyr	Gelation time
GelHA-0.30-αGlc	Gel-Tyr-αGlc	1	0.30	2 min 15 s
GelHA-0.45-αGlc	Gel-Tyr-αGlc	1	0.45	1 min 50 s
GelHA-0.30-βGal	Gel-Tyr-βGal	1	0.30	2 min 45 s
GelHA-0.45-βGal	Gel-Tyr-βGal	1	0.45	1 min 25 s
GelHA-0.30	Gel-Tyr	1	0.30	2 min
GelHA-0.45	Gel-Tyr	1	0.45	45 s

Table 3 Minimum (min), maximum (max) and mean diameter values, standard deviation (SD) and analysis of multiple comparisons performed with Tukey's method on SEM images; means which do not share a letter are significantly different

Formulation	Min [μm]	Max [μm]	Mean [μm]	SD [μm]	Groups
GelHA-0.30	316.72	540.5	421.18	77.31	A
GelHA-0.45	162.68	561.78	404.18	108.99	A
GelHA-0.45-αGlc	41.76	352.25	166.19	99.79	B
GelHA-0.30-βGal	29.07	307.64	129.98	87.26	B
GelHA-0.45-βGal	29.99	200.5	86.46	56.29	B
GelHA-0.30-αGlc	33.45	228.59	83.38	62.65	B

GelHA-0.45-αGlc formulations, indicating greater viscosity in hydrogels with lower Gel equivalents. Across all formulations, the n values were below 1, consistent with the shear-thinning behaviour qualitatively noted earlier. A slight increase in n was noted in formulations with higher Gel content, whereas lower n values were found in glucose and galactose conjugated hydrogels, reflecting their more pronounced shear-thinning behaviour.

A frequency sweep test was done to evaluate the mechanical stability of the formulations across a range of frequencies, with the G^* and $\tan\delta$ parameters reported in Fig. 6C and Table 5. G^* was higher in formulations with increased HA content and in hydrogels lacking sugar conjugation, supporting the results from the amplitude sweep test. Among the glyco-conjugated formulations,
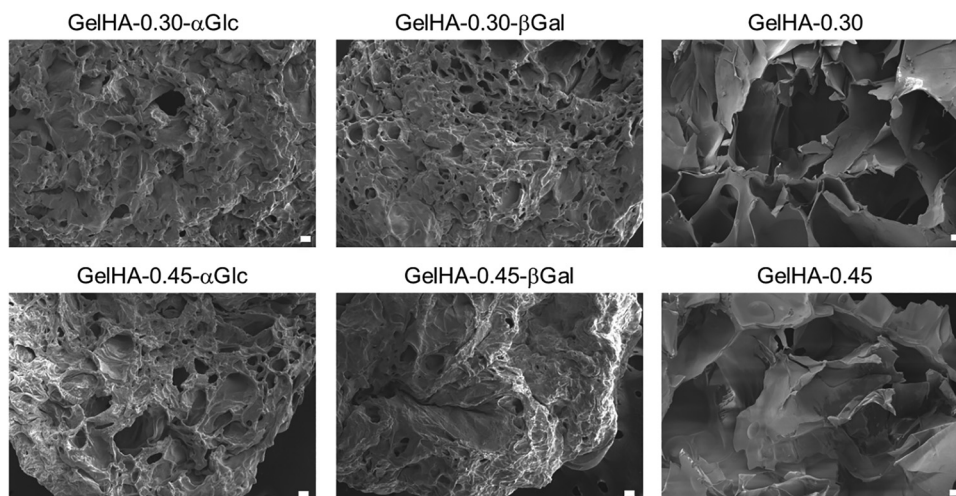

Fig. 5 SEM images of hydrogels cross-sections, 100× magnification, scale bar: 100 μm.
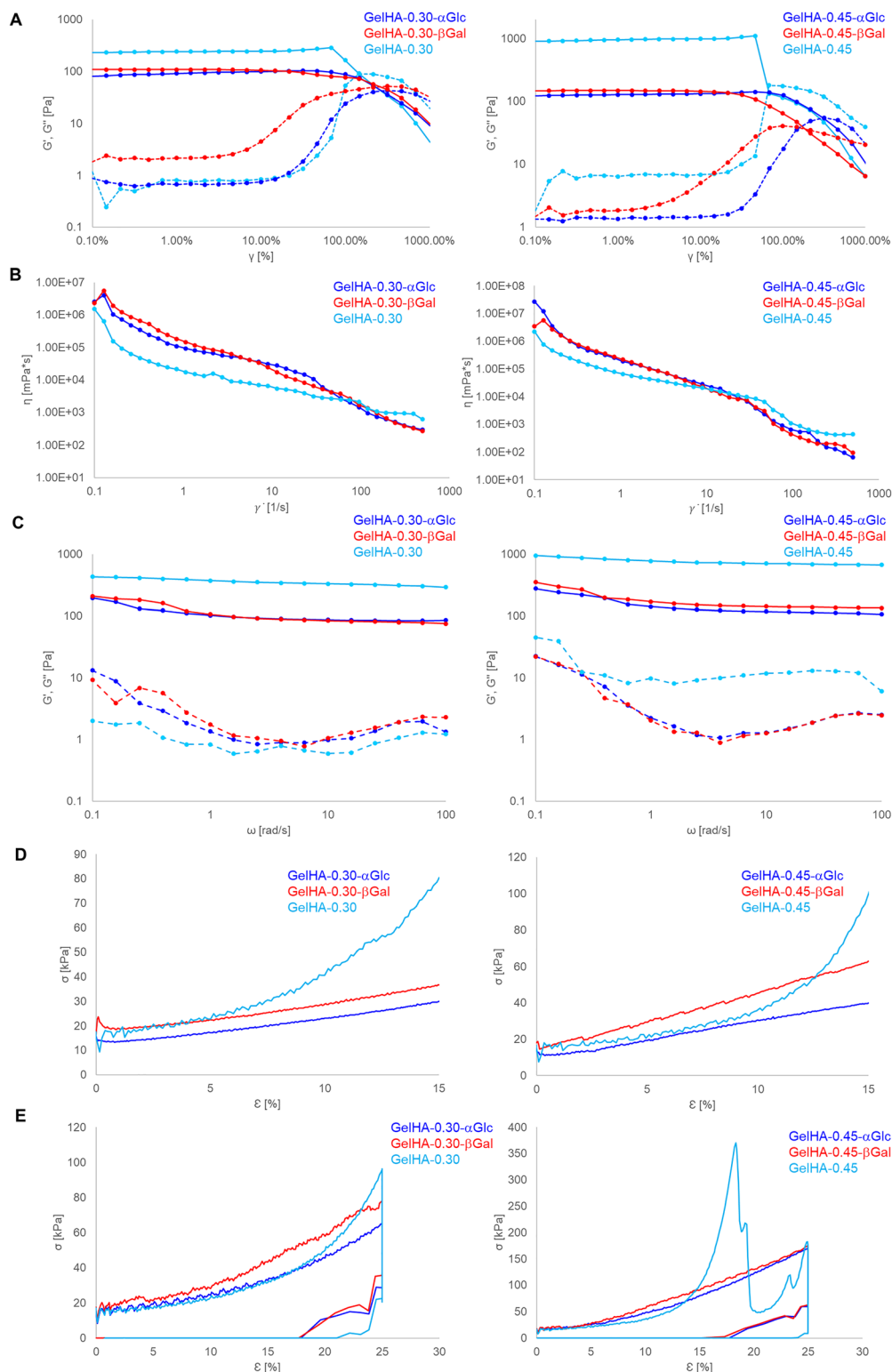
Fig. 6 G' (continuous line) and G'' (dashed line) curves of formulations obtained after amplitude sweep test (A), viscosity curves (B), G' (continuous line) and G'' (dashed line) curves of formulations obtained after frequency sweep test (C), stress–strain curves obtained from compression until 15% deformation (D) and compression until 25% deformation, 10s hold and unload tests (E).

those containing galactose showed consistently higher G^* values, regardless of the equivalents of Gel or HA. Concerning $\tan\delta$, all formulations exhibited values well below 1, indicating dominant elastic behaviour. Hydrogels without sugar conjugation displayed the lowest $\tan\delta$ values, suggesting that glyco-conjugation slightly increases the viscous component of the material.

© 2025 The Author(s). Published by the Royal Society of Chemistry

RSC Chem. Biol., 2025, **6**, 1893–1908 | **1899**

Table 4 Rheological parameters obtained after amplitude sweep test

Formulation	G' [Pa]	G'' [Pa]	γ_y [%]	γ_F [%]
GelHA-0.30-αGlc	93.0	1	85	214
GelHA-0.30-βGal	107.2	2.4	105	290
GelHA-0.30	244.4	0.9	90	148
GelHA-0.45-αGlc	129.1	1.6	100	260
GelHA-0.45-βGal	146.5	2.3	50	220
GelHA-0.45	965.9	6.4	70	85

Table 5 Rheological parameters obtained after viscosity curves, analysis with Power law and frequency sweep test. K is the consistency index, directly correlated to viscosity, and n is the flux index. n measures the pseudoplasticity of the material, and is 1 in Newtonian fluids, lower than 1 in shear thinning hydrogels and upper than 1 in shear thickening materials. When n is near 0, the material has a very strong shear thinning behaviour, because viscosity diminishes a lot when deformation rate increases, and $n = 0$ indicates the ideal case

Formulation	n	K [Pa·s^n]	G^* [Pa]	$\tan\delta$
GelHA-0.30-αGlc	0.094	162.9	106.8	0.021
GelHA-0.30-βGal	0.104	220.0	113.3	0.022
GelHA-0.30	0.328	32.1	356.5	0.003
GelHA-0.45-αGlc	0.073	209.6	150.4	0.027
GelHA-0.45-βGal	0.003	229.4	181.6	0.021
GelHA-0.45	0.110	98.8	763.5	0.018

Mechanical properties

Compression test was performed on cylindrical hydrogel specimens to evaluate their mechanical properties, with key parameters presented in Fig. 6D and E and Table 6. The initial elastic region of the stress–strain curve was analysed to determine the Young's modulus for each formulation. The highest stiffness values were observed in formulations without sugar conjugation (2.3 kPa for G_0.3H and 2.8 kPa for GelHA-0.45 as well as in GelHA-0.45-βGal, which exhibited a maximum of 3.1 kPa. A trend of increasing Young's modulus with higher HA content was noted, likely due to the higher phenol DoF in HA compared to Gel, which enhances crosslinking density. Despite the greater stiffness of formulations grafted only with tyramine, these hydrogels reached their yield points at lower deformations, indicating earlier onset of microstructural damage. This trend was further supported by hysteresis area analysis, which showed that GelHA-0.30 approached the fracture threshold, while GelHA-0.45 failed at 18.4% deformation. Across all formulations, a decline in stress was observed during the 10-second hold phase, consistent with viscoelastic relaxation. Upon unloading, the

materials exhibited only partial recovery, with evident residual deformation, suggesting microscale structural damage. Hydrogels modified with α-D-glucopyranose, β-D-galactopyranose displayed similar yield points, stress at 25% strain, and hysteresis percentages.

Correlation between rheological and mechanical parameters. A multivariate analysis was conducted to explore correlations and relationships among the mechanical and rheological parameters across all the formulations. Parameters included in this study were G^*, $\tan\delta$, n, K, γ_y and γ_F for the rheology and E, ε_y, σ_y, $\sigma_{25\%}$ and % hysteresis at $\varepsilon = 25\%$ for compression test. A heatmap correlation matrix was generated based on standardized values of these key parameters to provide a qualitative overview of parameter distribution and similarity among formulations (Fig. 7A). Stronger positive correlations were found between $\sigma_{25\%}$ and % hysteresis ($R^2 = 0.98$), K and $\tan\delta$ ($R^2 = 0.87$), ε_y and K ($R^2 = 0.86$), E and $\sigma_{25\%}$ ($R^2 = 0.82$). Principal component analysis (PCA) was subsequently performed to reduce dimensionality and quantitatively determine the main sources of variation within the dataset (Fig. 7B). Principal dimension 1 (PC1) accounts for 47.1% of the total variance, while principal dimension 2 (PC2) explains 37.8%, together capturing 84.9% of the total variability in the dataset. The relative positioning of hydrogel formulations reflects distinct material behaviours, while the direction and magnitude of the variable vectors indicate their contribution and correlation. PCA revealed that PC1 is mainly influenced by variables such as G^*, n% hysteresis, E and $\sigma_{25\%}$, which are associated with the structural and viscoelastic differences among the various hydrogel formulations. In contrast, PC2 is more affected by K, ε_y, γ_y and γ_F, reflecting secondary characteristics related to deformation and flow behaviour. Formulation GelHA-0.3 is placed in the upper-right quadrant, indicating high pseudoplastic behaviour along with a more rigid and organized structure. Conversely, GelHA-0.45 appears in the lower-right quadrant, aligned with vectors E and G^*, suggesting increased elasticity and rigidity, but also greater energy dissipation and reduced mechanical energy retention. For the sugar-modified hydrogels, GelHA-0.3-αGlc and GelHA-0.3-βGal cluster in the upper-left quadrant, showing good deformability and moderate viscoelastic properties. Among them, GelHA-0.3-αGlc demonstrates higher consistency and intermediate mechanical behaviour. In contrast, GelHA-0.45-αGlc and GelHA-0.45-βGal are found in the lower-left quadrant, indicating a weaker structure with more viscous and dissipative characteristics.

Since parameters $\sigma_{25\%}$ and % hysteresis exhibited highest R^2 value, they were modelized through a linear regression (SI). Three multiple linear regression analyses were conducted to

Table 6 Mechanical parameters obtained from compression tests

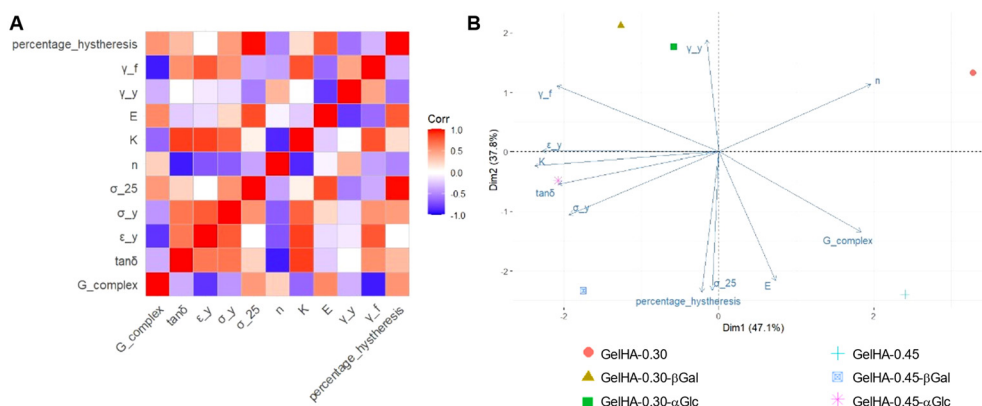|	GelHA-0.30-αGlc	GelHA-0.30-βGal	GelHA-0.30	GelHA-0.45-αGlc	GelHA-0.45-βGal	GelHA-0.45
E [kPa]	1.2	1.1	2.3	2.0	3.1	2.8
ε_y [%]	16.9	15.4	10.6	17.7	19.6	9.2
σ_y [kPa]	36.4	44.1	23.1	99.2	87.7	31.5
$\sigma_{25\%}$ [kPa]	64.8	74.3	95.7	161.0	163.5	174.8
ε_r [%]	—	—	—	—	—	370.2
σ_r [kPa]	—	—	—	—	—	18.4
% hysteresis at $\varepsilon = 25\%$	87.5	88.8	96.1	87.6	87.8	99.0

Fig. 7 Heatmap correlation matrix of rheological and mechanical key parameters (A) and PCA performed on formulations and parameters (B).

investigate how combinations of mechanical and rheological parameters influence the overall properties of the hydrogels. K was selected as the dependant variable of the multiple regression because it is a macroscopic measure of the viscoelastic behaviour of hydrogels and their inner structural interaction, which is influenced by composition, crosslinking density and links distribution. Its variation is highly sensitive to structural modifications thus it is a good target to evaluate the influence of more predictive parameters. The first model included n and % hysteresis as independent variables to assess whether viscoelasticity is influenced by both shear-thinning behaviour and hysteresis. The model yielded a multiple R^2 of 0.837 and a p-value of 0.066, suggesting a relatively strong relationship, although not statistically significant at the 0.05 threshold. The second model used G^* and ε_y to explore the association between hydrogel stiffness and the capacity for plastic deformation before fracture. This model resulted in a multiple R^2 of 0.765 and a p-value of 0.114, indicating a weaker correlation compared to the first. The third model involved E and $\sigma_{25\%}$ as predictors to examine the relationship between structural resistance under load and the initial stiffness of the material. In this case, the multiple R^2 and p-value were 0.299 and 0.586, respectively, highlighting a poor fit and a weak association between the selected parameters. Among the three, viscoelastic behaviour was best described by the first model (n and % hysteresis). However, diagnostic plots revealed several issues with this model, including non-linearity, heteroscedasticity, and non-normality of residuals (SI). To address these limitations,

the initial linear model was compared with three alternative models: a log-transformed, a robust regression, and a square root-transformed model. Based on the Akaike Information Criterion (AIC), the log-transformed model was selected as the most appropriate, yielding an improved R^2 of 0.937 (SI). This result indicates that the logarithmic transformation improved the overall model performance by reducing the influence of heteroscedasticity.

Cellular test

hBM-MSCs were seeded in hydrogels and cultured for 21 days to evaluate cell viability and morphological changes induced by sugar conjugation, using formulations grafted only with tyramine as controls. The resulting images are presented in SI.

During the first three days, hydrogels did not induce significant morphological changes. However, by day 7, some differences began to emerge. In control hydrogels, only a few cells started to elongate, while the majority remained rounded. In other formulations, particularly those with α-D-glucopyranose, a greater number of cells elongated. These differences became more pronounced over time. By day 21, hydrogels with galactose showed a high number of elongated cells. In the presence of glucose, all cells elongated, forming a dense pellet. In control hydrogels, both rounded and elongated cells were observed. When comparing formulations with varying concentrations of Gel and HA, in presence of sugars cells tend to form more aggregates and proliferate more. However, in control materials, a higher number of elongated cells were present in GelHA-0.45.
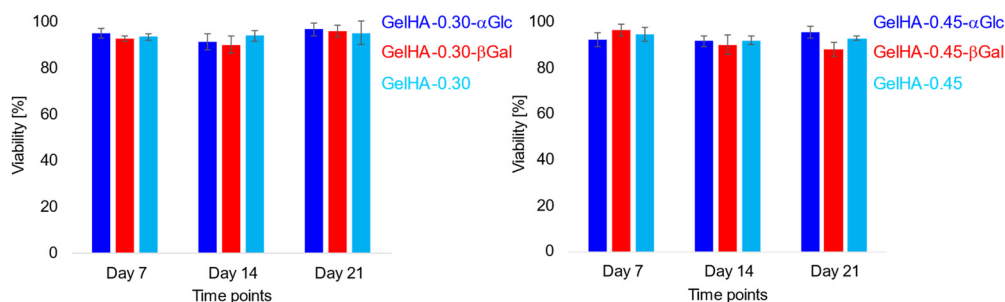

Fig. 8 Viability calculated with live−dead assay with standard deviation (SD) error bars.

The percentage viability was calculated for all formulations (Fig. 8), demonstrating optimal cytocompatibility, with all results greater than 85%. One-way ANOVA revealed no significant differences among all formulations at three time points (SI).

Fig. 9A shows the fluorescent images of cells labelled with Phalloidin and DAPI, in which morphological trends observed below were confirmed. Cells included in formulations containing glucose and galactose, particularly GelHA-0.30-αGlc and GelHA-0.45-αGlc, exhibited a more elongated morphology compared to controls. Nuclei roundness was quantified with Fiji ImageJ, and the resulting violin plot is shown in Fig. 9B. In formulations with glucose and galactose nuclei appear more elongated than in control samples, with roundness values of 0.50 (GelHA-0.30-αGlc), 0.57 (GelHA-0.30-βGal), 0.62 (GelHA-0.45-αGlc), and 0.53 (GelHA-0.45-βGal). Control samples, GelHA-0.30 and GelHA-0.45HA, exhibited slightly higher roundness values of 0.71 and 0.70, respectively.

Lectin assay

The cell N- and O-glycosylation patterns are highly context-dependent, influenced by the specific tissue in which they are expressed, the availability of nucleotide-sugar donors, the expression levels of glycosylation-related enzymes, and the competition among these enzymes for shared substrates. Moreover, it is well established that changes in the cellular microenvironment can rapidly alter glycan profiles.[20–22] To evaluate if glycosylation of ECM mimics impact on the modulation of cell glycoprofiles, lectin staining was performed on 50 μm fixed hydrogels slices to assess protein glycosylation. Four lectins were selected to characterize the effect of differentially glycosylated hydrogels: Concanavalin A. (Con A) which recognize specifically αGlc[23] and α-D-mannose (αMan) particularly in high mannose residues; Erythrina cristagalli lectin (ECL) used to detect βGal with a strong preference for Galβ1-4/3GlcNAc residues;[24] Aleuria aurantia lectin (AAL) which recognizes fucose linked (α-1,6) to N-acetylglucosamine or (α-1,3) to N-

acetyllactosamine typically produced by hBM-MSCs;[25] and Maackia amurensis Lectin (MAL II) which recognises sialic acid residues in an (α-2,3) linkage to galactose.[26] The results are presented in Fig. 10. The first column displays the combined staining of Con A and DAPI. Formulations containing αGlc show a higher signal intensity compared to other samples, indicating increased αGlc production by hBM-MSCs. Additionally, the GelHA-0.30-βGal and GelHA-0.45-βGal formulations exhibit greater ConA recognition than the non-glycosylated hydrogels. The second column of Fig. 10 shows ECL staining. A stronger ECL signal is observed in formulations containing βGal, whereas formulations with αGlc do not exhibit a statistically significant difference compared to the control hydrogel. The third column shows the results of AAL staining, used to determine whether hBM-MSCs expressed fucosylated glycans after 21 days of culture. A stronger AAL signal is observed in the formulations containing αGlc, indicating increased fucose expression. This signal is also more pronounced in the βGal containing hydrogels compared to the control formulations. Finally, the fourth column displays MAL II staining, performed to assess the expression of sialic acid by hBM-MSCs. As with AAL, hydrogels functionalized with sugars exhibit higher MAL II signals, with no statistically significant differences between formulations with αGlc and βGal. However, in this case, the differences are less distinct, as cells in the unmodified GelHA-0.30 and GelHA-0.45 hydrogels also show MAL II staining, though not as strong as in the sugar-conjugated formulations. Fig. 11 displays bar plots showing the percentage of each lectin detected, normalized to cell count, with statistical significance assessed by ANOVA followed by Tukey's *post hoc* test. Lectin-specific comparisons across different sample types are shown, while comparisons of different lectins within the same hydrogel type are provided in the SI. Interestingly the formulations containing αGlc and those containing βGal both showed significant fucosylation and sialylation. While the role of fucosylation in cell adhesion and signalling is well established, its
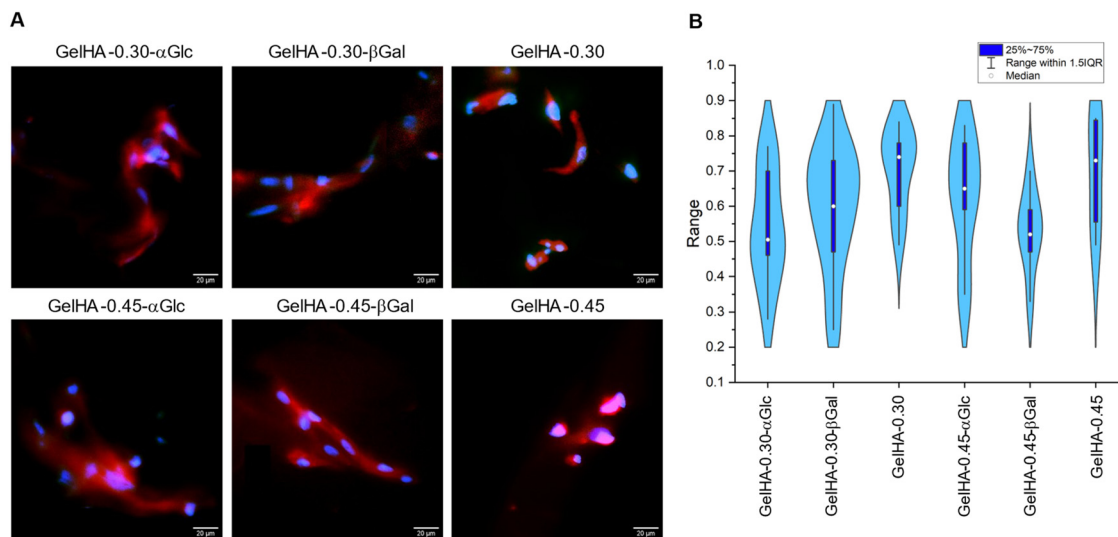

Fig. 9 Morphological characterization on hydrogels performed with Phalloidin–DAPI (A) and nuclei roundness violin plot (B). Scale bar: 20 μm.
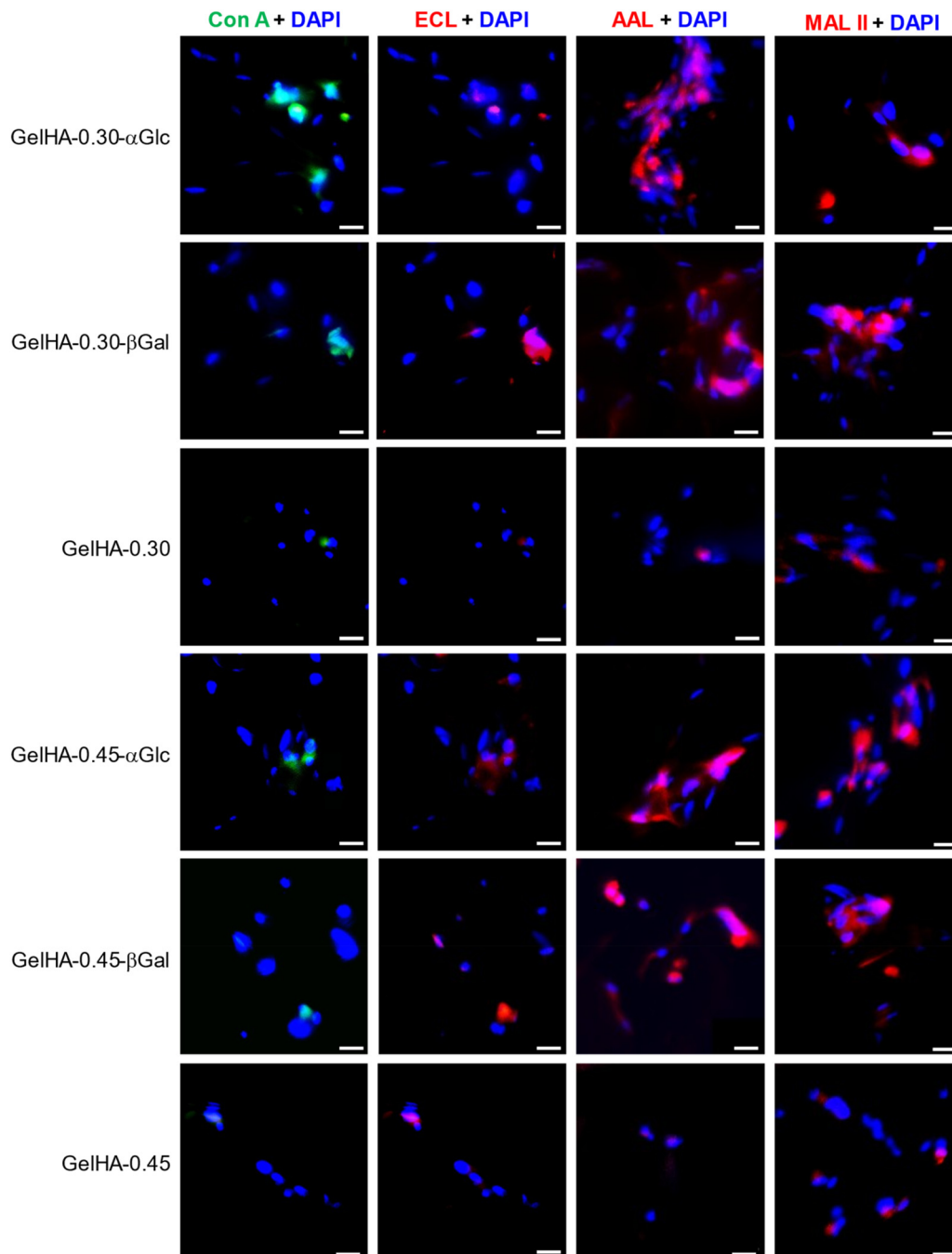
Fig. 10 Lectin assay performed on hydrogels, using Con A (first column), ECL (second column), AAL (third column) and MAL II (fourth column) in combination with DAPi to visualize nuclei, scale bar: 20 μm.

impact on BM-MSCs is still under investigation.[27] In the present study, it was not possible to clearly distinguish between N- and O-linked glycosylation; however, it is known that MAL II preferentially recognizes O-linked glycans. Sialylation is a critical process for preserving the stem cell population in the body. In particular, the expression of α2-3-sialylated glycans on MSCs has been implicated in the regulation of cell adhesion and migration.[28] In this context, the increased MAL II binding observed in glycosylated samples suggests a higher expression of α2-3-sialylated structures in hBM-MSCs, potentially reflecting an enhanced migratory potential. Rebelo *et al.* reported a correlation between glucose conjugation and an increase in produced sialic acid, a finding that is supported by our data.[20] However, unlike their study, we also observed an increase in sialic acid production in formulations containing βGal. We can conclude that, as previously reported for other cell types, specific neo-glycosylation of ECM mimics significantly influences cell glycosylation (Table 7).
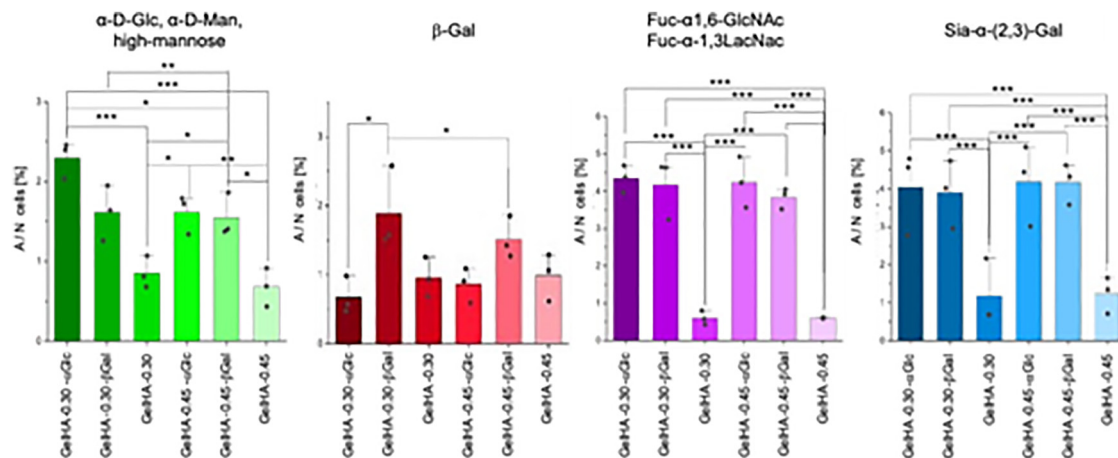
© 2025 The Author(s). Published by the Royal Society of Chemistry

RSC Chem. Biol., 2025, **6**, 1893–1908 | **1903**

Fig. 11 Bar plots formulated for each lectin type, with results expressed as mean $\pm$ SD. Statistical analysis was performed using one-way ANOVA followed by Tukey's *post hoc* test to assess significance. Asterisks indicate levels of statistical significance as follows: "***" for p-value < 0.001, "**" for $0.001 \leq p$-value < 0.01, and "*" for $0.01 \leq p$-value < 0.05.

Immunofluorescence assay

Immunofluorescence is a widely used technique to visualize specific proteins within cells and tissues, providing spatial information on their localization and expression.[29] The evaluating of adhesion, signalling, and matrix-remodelling markers can be indicative of MSC functional state in 3D matrices.[30–32] Therefore, 50 µm fixed hydrogel slices were first treated with a 2% w/v BSA blocking solution for 1 h, followed by incubation with four different primary antibodies for 3 h at room temperature. Secondary fluorescent antibodies were then applied to enable visualization. Nestin, β-catenin, MMP-2, MMP-9 were selected to evaluate the impact of hydrogel glycosylation on MSC modulation. Nestin was used to identify functional hBM-MSCs, as it is associated with high proliferative and migratory potential, both fundamental for tissue repair and for creating niches that support other stem cells.[33–35] β-catenin was included because it plays a central role in maintaining the undifferentiated state of hBM-MSCs, enabling them to self-renew, proliferate, and differentiate into specialized cell types such as osteogenic, adipogenic, and chondrogenic lineages. This reflects the importance of the Wnt/β-catenin signalling pathway, a key regulator of MSC fate and stem cell maintenance.[36–38] MMP-2 was selected for its involvement in cell migration as well as its role in modulating hBM-MSC differentiation; notably, elevated MMP-2 expression has been linked to chondrogenic differentiation, making it a potential marker of chondrogenesis.[39,40] Finally, MMP-9 expression was evaluated, although its relevance is less favourable, as MSC-derived MMP-9 has been implicated in promoting lung cancer progression and metastasis by enhancing epithelial-to-mesenchymal transition and cell invasiveness.[41] Results are presented in Fig. 12, where DAPI staining was used to visualize cell nuclei. Statistical analysis was performed using ANOVA with multiple comparisons to highlight significant differences (Fig. 13 and SI). Nestin was expressed in all samples, with increased levels in βGal-containing hydrogels and reduced levels in αGlc-containing hydrogels, although these variations showed low statistical significance. Given that Nestin is associated with proliferation and niche formation, its upregulation in βGal samples suggests a positive effect, despite its presence across all groups. For β-catenin, both sugar-conjugated formulations showed increased expression, more pronounced in αGlc samples, indicating a potential role in maintaining the undifferentiated state of hBM-MSCs and preventing senescence. In contrast, MMP-2 expression was higher in βGal samples, though both sugar-conjugated groups showed an overall increase. Since MMP-2 secretion is linked to differentiation, particularly chondrogenesis, these findings suggest that βGal promotes hBM-MSC differentiation. Finally, MMP-9 expression was absent in all samples, with no changes observed upon sugar conjugation. This absence is favourable, as MMP-9 secretion is typically associated with cancer-related differentiation processes and metastatic potential. When comparing hydrogels with identical sugar composition but varying gelatin and HA concentrations, only minor differences in marker expression were observed, with slightly higher levels in

Table 7 Summary of the changes seen in the expression of different sugar residues in the presence of the different hydrogels measured through the binding of different lectins, in comparison to the control (GelHA without glycosylation), where "↑↑" indicates a strong change, "↑" a moderate change and "=" denotes no significative change

Group	α-D-Glc, α-D-Man, high-mannose (binding of Con A)	β-Gal (binding of ECL)	Fuc-α1,6-GlcNAc or Fuc-α-1,3LacNac (binding of AAL)	Sia(α2-3)-Gal (binding of MAL II)
GelHA- αGlc	↑↑	=	↑↑	↑↑
GelHA- βGal	↑	↑	↑↑	↑↑

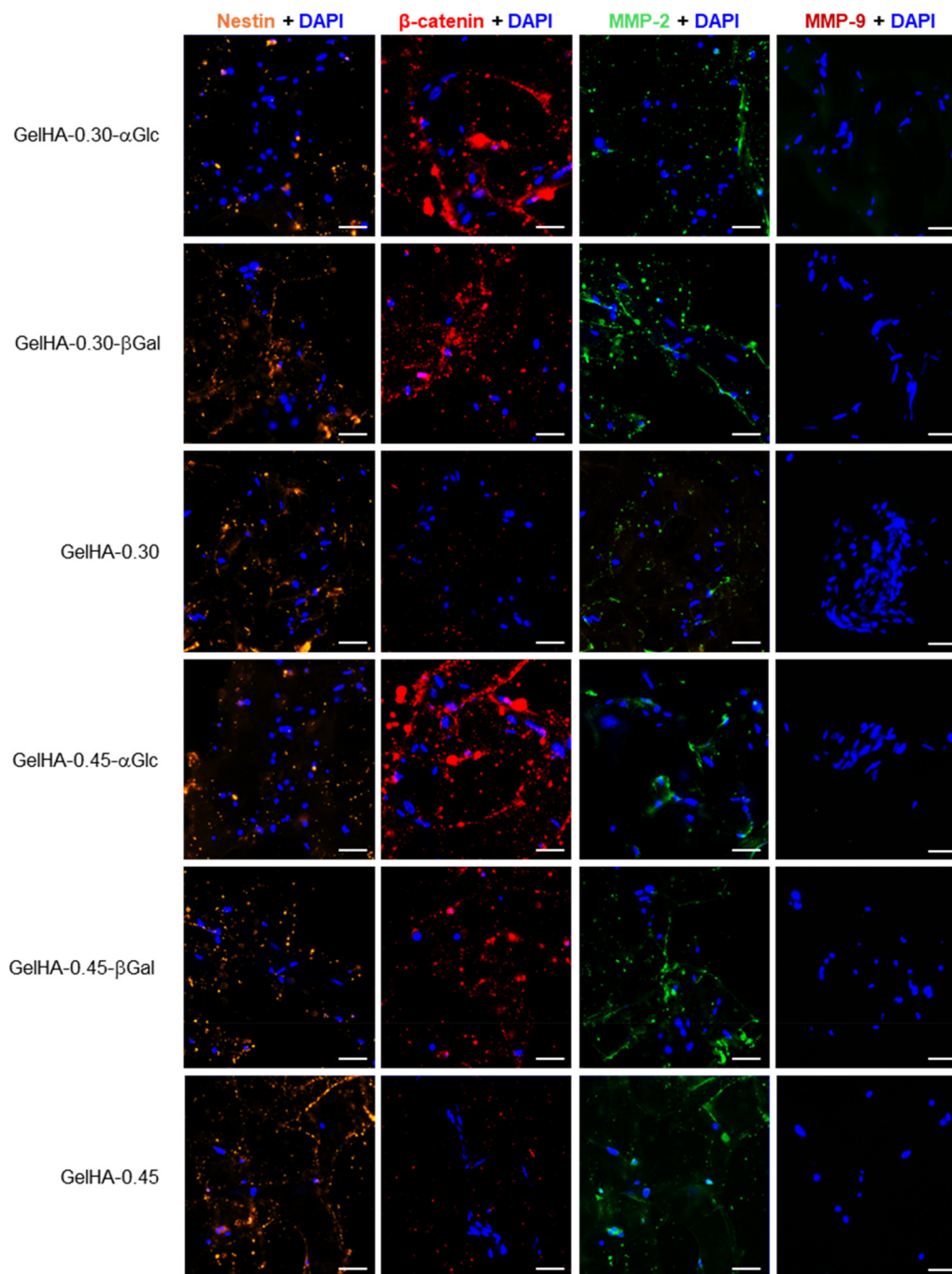© 2025 The Author(s). Published by the Royal Society of Chemistry

Fig. 12 Immunofluorescence staining for Nestin (first column), β-catenin (second column), MMP-2 (third column), and MMP-9 (fourth column), with DAPI used to visualize nuclei. Scale bar: 50 μm.

hydrogels containing more gelatin. These variations were not statistically significant, indicating that changes in the protein or polysaccharide content of the matrix exert a limited effect on cellular behaviour. In contrast, the type of glycan incorporated into the hydrogel emerged as the primary factor influencing hBM-MSC expression. This finding underscores the critical role of glycan composition in modulating cell responses, suggesting that glycan identity, rather than matrix concentration, is the dominant determinant of proliferation and

differentiation potential within these hydrogel systems, as shown in Table 8.

Mechanistic discussion

The mechanistic effects of glycan conjugation were further investigated through additional quantitative analyses to clarify the influence of α- *versus* β-glycans on cellular responses. As observed, both the amounts of Gel and HA, as well as glycan conjugation, affect the mechanical and rheological properties
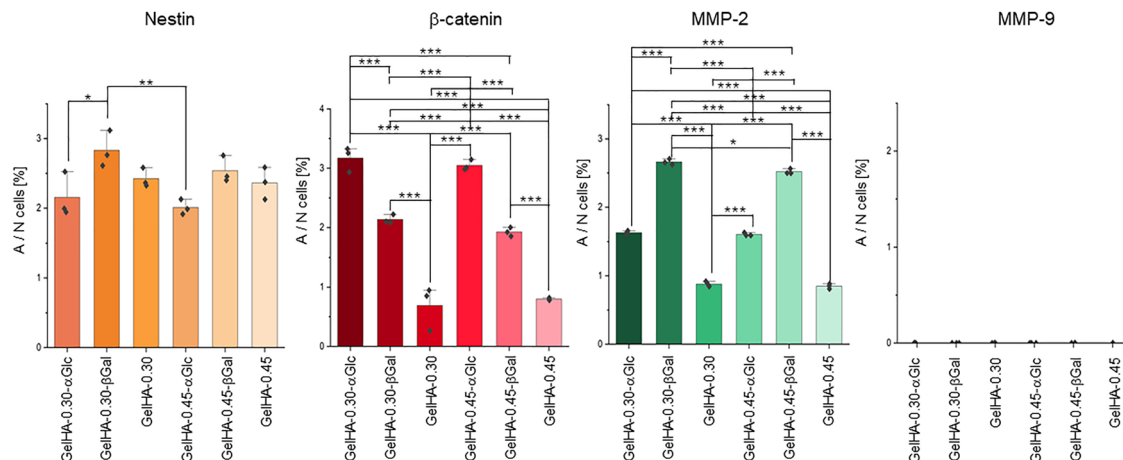
Fig. 13 Bar plots formulated for each antibody type excluding MMP-9 which was no detected in all samples, with results expressed as mean $\pm$ SD. Statistical analysis was performed using one-way ANOVA followed by Tukey's *post hoc* test to assess significance. Asterisks indicate levels of statistical significance as follows: "***" for p-value < 0.001, "**" for $0.001 \leq p$-value < 0.01, and "*" for $0.01 \leq p$-value < 0.05.

Table 8 Summary of the changes seen in the binding of different antibodies the presence of the different hydrogels, in comparison to the control (GelHA without glycosylation), where "↑↑" indicates a strong change, "↑" a moderate change and "=" denotes no significative change

Group	Nestin	β-catenin	MMP-2	MMP-9
GelHA-αGlc	↓	↑↑	↑	=
GelHA-βGal	↑	↑	↑↑	=

of the hydrogels. Qualitatively, a lower correlation was observed between E and cell roundness after 21 days of culture. However, lower roundness was consistently seen in glycan-conjugated formulations, suggesting that cell elongation is more sensitive to glycan grafting than to E. While E is generally recognized as a key determinant of cell fate,[42] in this case the hydrogels were mechanically very similar, providing insufficient variation in E to allow a strong significant mechanical signal. Furthermore, formulations with identical Gel conjugation but varying Gel and HA content showed more similar cell roundness than comparisons between formulations with and without glycan conjugation, indicating that glycan presence is the primary factor influencing cell elongation. No significant differences in cell roundness were observed between α- and β-glycans, although lectin and immunofluorescence assays revealed some variations. Overall, glycan conjugation resulted in higher lectin expression compared to controls, while formulations with identical sugar conjugation but different gelatin and HA concentrations showed no substantial differences. This indicates that glycan conjugation is a more decisive factor in modulating the cellular microenvironment than stiffness or biomaterial composition. Specifically, AAL and MAL II showed comparable expression for α- and β-glycans, whereas ConA expression was higher with α-glycan conjugation and ECL expression was higher with β-glycan conjugation. These differences are particularly relevant, as they are linked to signalling pathways that influence cell fate. Consistently, immunofluorescence analysis

revealed variations in Nestin, β-catenin, and MMP-2 expression depending on the type of glycan conjugation, while no significant differences were observed in hydrogels with the same sugar conjugation but different gelatin and HA content.

Random forest analysis was applied to evaluate the relative contribution of material and biochemical parameters in shaping cellular responses. Random Forest is an ensemble machine learning (ML) method that combines the predictions of multiple decision trees to improve accuracy and reduce overfitting. In this approach, each tree is trained on a bootstrap sample of the dataset and splits are made on randomly selected subsets of variables, thereby decorrelating the trees and enhancing robustness.[43,44]

In this study, the model was used in a regression framework, where the outcome variables were quantitative descriptors of cell behaviour (nuclear roundness, lectin binding and integrin expression), and the predictors included both mechanical and compositional parameters: E, gelatin and HA content and glycan type (α- *vs.* β-glycans or control). Variable importance was evaluated using two measures: the percent increase in mean squared error (%IncMSE), which shows how much model accuracy decreases if a variable is randomized, and the increase in node purity (IncNodePurity), which indicates how strongly each variable helps the model explain variation in the data. This analysis identified the parameters with the greatest impact on cellular outcomes. Glycan type emerged as the dominant predictor, with K also contributing strongly, while E had a moderate effect. In contrast, gelatin and HA content showed minimal or even negative predictive value, suggesting that overall material composition was less influential than glycan conjugation in modulating cell behaviour (SI).

Conclusions

In this study a strategy to develop glyco-functionalised hydrogels with tailored properties is proposed. The modular

1906 | *RSC Chem. Biol.*, 2025, **6**, 1893–1908

© 2025 The Author(s). Published by the Royal Society of Chemistry

approach, based on the oxidative HRP crosslinking of tyramine-functionalised gelatin and hyaluronic acid, was exploited with gelatin functionalised with αGlc and βGal providing relevant signalling in BM-MSC microenvironment. The influence of each formulation was thoroughly characterized in terms of chemical composition, rheological behaviour, and mechanical properties to assess the influence of Gel, HA, and glyco-conjugated components. Crosslinking through phenol groups was comparable across all formulations, as tyramine grafting levels were similar among the glycofunctionalized gelatins. Glyco-functionalized hydrogels exhibited reduced rigidity and increased capacity for deformation prior to micro-rupture and overall failure, likely attributable to their higher viscosity. Formulations containing αGlc and βGal displayed similar mechanical behaviour to each other. Biological evaluation of hydrogel and glycosylated hydrogel with BM-MSC highlighted the effect of differential hydrogel glycosylation on cell response under growth factor-free conditions. Cells cultured in 3D in glycosylated hydrogels displayed higher viability and more elongated morphology, with evidence of altered glycosylation profiles compared to not-glycsosylated controls. Furthermore, in αGlc hydrogels, hBM-MSCs showed increased β-catenin and MMP-2 expression, whereas MMP-9 was not detectable. These data are consistent with a pre-remodelling phenotype, without detectable tumorigenics markers. These findings indicate that glycan identity in the ECM microenvironment are dominant drivers of MSC modulation. Together, these results support glycan engineering of ECM mimics as a modular route to tailor cell behaviour, with glycan identity emerging as a stronger determinant for cell fate modulation. Given the inherent heterogeneity of human body tissues, the ability to tailor and combine these hydrogels offers a promising strategy to more accurately mimic native tissue architecture and functionality.

Conflicts of interest

There are no conflicts to declare.

Data availability

All data supporting the findings of this study, including raw and processed datasets, microscopy images, and analysis scripts, have been deposited in Zenodo and are publicly available at DOI: **https://doi.org/10.5281/zenodo.17251564**.

Supplementary information (SI) is available. See DOI: **https://doi.org/10.1039/d5cb00185d**.

Acknowledgements

References

1 J. Nicolas, S. Magli, L. Rabbachin, S. Sampaolesi, F. Nicotra and L. Russo, *Biomacromolecules*, 2020, **21**, 1968–1994.

2 U.S. Food & Drug Administration, FDA Announces Plan to Phase Out Animal Testing Requirement for Monoclonal Antibodies and Other Drugs.

3 Y. Zhao, M. Takahashi, J. Gu, E. Miyoshi, A. Matsumoto, S. Kitazume and N. Taniguchi, *Cancer Sci.*, 2008, **99**, 1304–1310.

4 C. Gardelli, L. Russo, L. Cipolla, M. Moro, F. Andriani, O. Rondinone, F. Nicotra, G. Sozzi, G. Bertolini and L. Roz, *Cancer Sci.*, 2021, **112**, 217–230.

5 T. Hennet, *Curr. Opin. Struct. Biol.*, 2019, **56**, 131–138.

6 I. Tvaroška, *Molecules*, 2024, **29**, 1417.

7 S. Gunasekaran, *Biomed. Mater. & Devices*, 2024, **2**, 307–315.

8 S. Miyata and H. Kitagawa, *Biochim. Biophys. Acta, Gen. Subj.*, 2017, **1861**, 2420–2434.

9 P. Kastana, E. Choleva, E. Poimenidi, N. Karamanos, K. Sugahara and E. Papadimitriou, *FEBS J.*, 2019, **286**, 2921–2936.

10 S. Haylock-Jacobs, M. B. Keough, L. Lau and V. W. Yong, *Autoimmun. Rev.*, 2011, **10**, 766–772.

11 Z. Guo, G. M. Salamonczyk, K. Han, K. Machiya and C. J. Sih, *J. Org. Chem.*, 1997, **62**, 6700–6701.

12 L. Russo, A. Gautieri, M. Raspanti, F. Taraballi, F. Nicotra, S. Vesentini and L. Cipolla, *Carbohydr. Res.*, 2014, **389**, 12–17.

13 L. Russo, A. Sgambato, M. Lecchi, V. Pastori, M. Raspanti, A. Natalello, S. M. Doglia, F. Nicotra and L. Cipolla, *ACS Chem. Neurosci.*, 2014, **5**, 261–265.

14 M. Bracchi, F. Nicotra and L. Russo, *Carbohydr. Polym. Technol. Appl.*, 2025, **11**, 100928.

15 P. Guerrero, I. Zugasti, A. Etxabide, H. N. D. Bao, T. Trang Si, M. Peñalba and K. de la Caba, *Polymers*, 2020, **12**, 570.

16 J. Hou, C. Li, Y. Guan, Y. Zhang and X. X. Zhu, *Polym. Chem.*, 2015, **6**, 2204–2213.

17 J. Hernández-Ruiz, M. B. Arnao, A. N. P. Hiner, F. García-Cánovas and M. Acosta, *Biochem. J.*, 2001, **354**, 107.

18 R. Naranjo-Alcazar, S. Bendix, T. Groth and G. Gallego Ferrer, *Gels*, 2023, **9**, 230.

19 B. Guo, *Applied Well Cementing Engineering*, Elsevier, 2021, pp. 253–290.

20 A. L. Rebelo, J. Bizeau, L. Russo and A. Pandit, *Biomacromolecules*, 2020, **21**, 2681–2694.

21 M. Tian, X. Li, L. Yu, J. Qian, X. Bai, J. Yang, R. Deng, C. Lu, H. Zhao and Y. Liu, *Cell Commun. Signaling*, 2025, **23**, 214.

22 M. He, X. Zhou and X. Wang, *Signal Transduct. Target Ther.*, 2024, **9**, 194.

23 S. Musleh, I. Alibay, P. C. Biggin and R. A. Bryce, *J. Chem. Inf. Model.*, 2024, **64**, 8063–8073.

24 K. Turton, *Glycobiology*, 2004, **14**, 923–929.

25 E. C. Adam, S. T. Holgate and P. M. Lackie, *Am. J. Physiol.: Lung Cell. Mol. Physiol.*, 2007, **292**, L462–L468.

© 2025 The Author(s). Published by the Royal Society of Chemistry

RSC Chem. Biol., 2025, **6**, 1893–1908 | **1907**

26 Y. Qin, Y. Chen, J. Yang, F. Wu, L. Zhao, F. Yang, P. Xue, Z. Shi, T. Song and C. Huang, *Sci. Rep.*, 2017, **7**, 46041.

27 G. Gaspari, A. Lange-Consiglio, F. Cremonesi and S. Desantis, *Int. J. Mol. Sci.*, 2025, **26**, 1784.

28 A. Heiskanen, T. Hirvonen, H. Salo, U. Impola, A. Olonen, A. Laitinen, S. Tiitinen, S. Natunen, O. Aitio, H. Miller-Podraza, M. Wuhrer, A. M. Deelder, J. Natunen, J. Laine, P. Lehenkari, J. Saarinen, T. Satomaa and L. Valmu, *Glycoconj. J.*, 2009, **26**, 367–384.

29 I. D. Odell and D. Cook, *J. Invest. Dermatol.*, 2013, **133**, 1–4.

30 D. Cáceres-Calle, I. Torre-Cea, L. Marcos-Zazo, I. Carrera-Aguado, E. Guerra-Paes, P. Berlana-Galán, J. M. Muñoz-Félix and F. Sánchez-Juanes, *Int. J. Mol. Sci.*, 2025, **26**, 904.

31 M. R. Chastney, J. Kaivola, V.-M. Leppänen and J. Ivaska, *Nat. Rev. Mol. Cell Biol.*, 2025, **26**, 147–167.

32 A. Huttenlocher and A. R. Horwitz, *Cold Spring Harbor Perspect. Biol.*, 2011, **3**, a005074–a005074.

33 H. Wang, C. Jiang, J. Cai, Q. Lu, Y. Qiu, Y. Wang, Y. Huang, Y. Xiao, B. Wang, X. Wei, J. Shi, X. Lai, T. Wang, J. Wang and A. P. Xiang, *Life Med.*, 2022, **1**, 359–371.

34 L. Xie, X. Zeng, J. Hu and Q. Chen, *Stem Cells Int.*, 2015, **2015**, 1–9.

35 H. M. Lee, S.-R. Seo, J. Kim, M. K. Kim, H. Seo, K. S. Kim, Y.-J. Jang and C. J. Ryu, *Stem Cell Res. Ther.*, 2020, **11**, 210.

36 P. Dashti, E. A. Lewallen, G. S. Stein, B. C. J. van der Eerden, J. P. T. M. van Leeuwen and A. J. van Wijnen, *Biochem. Biophys. Rep.*, 2024, **40**, 101847.

37 Y. Badralmaa and V. Natarajan, *J. Biol. Chem.*, 2025, **301**, 108057.

38 M. D. Hoffman and D. S. W. Benoit, *J. Tissue Eng. Regen. Med.*, 2015, **9**, E13–E26.

39 Y. Arai, S. Park, B. Choi, K.-W. Ko, W. Choi, J.-M. Lee, D.-W. Han, H.-K. Park, I. Han, J. Lee and S.-H. Lee, *Int. J. Mol. Sci.*, 2016, **17**, 963.

40 F. Mannello, *Stem Cells*, 2006, **24**, 1904–1907.

41 J. J. Gu, J. Hoj, C. Rouse and A. M. Pendergast, *PLoS One*, 2020, **15**, e0241423.

42 A. Mishra, U. Modi, R. Sharma, D. Bhatia and R. Solanki, *Biomed. Eng. Adv.*, 2025, **9**, 100143.

43 V. Ignatenko, A. Surkov and S. Koltcov, *PeerJ Comput. Sci.*, 2024, **10**, e1775.

44 V. Y. Kulkarni and P. K. Sinha, in 2012 International Conference on Data Science & Engineering (ICDSE), IEEE, 2012, pp. 64–68.